ISSN1027-5495. Functional Materials, 32, No.1 (2025), p. 13-20
doi:http://dx.doi.org/10.15407/fm32.01.13 © 2025 — STC "Institute for Single Crystals"

Thermal stability of perovskites $CH_3NH_3PbX_3$ (X = Cl, Br, I)

S.S. Smolyak, V.L. Karbivskyy, V.Kh. Kasianenko, S.A. Nedilko, S.I. Shulyma, N.A.Kurgan, O.A. Puzko, L.I. Karbivska, A.P. Soroka

G.V. Kurdyumov Institute for Metal Physics of the National Academy of Sciences of Ukraine, blvd. Academician Vernadsky, 36, 03142 Kyiv, Ukraine

Received August 17, 2024

The morphology and structures of perovskites were investigated using scanning electron microscopy and X-ray diffraction methods. The samples exhibit a monophase structure. The thermal stability and degradation processes of a series of perovskites $CH_3NH_3PbX_3$ (where X = Cl, Br, I) were analyzed by the thermogravimetric method. The results indicate that the thermal stability is preserved up to 335°C for X = Cl, 330°C for X = Br, and 310°C for X = I. Additionally, a correlation was established between the thermal stability of $CH_3NH_3PbX_3$ perovskites and the characteristics of the halogen atom in their structure. It was concluded that the thermal stability of hybrid organic-inorganic perovskites can be adjusted by varying the halogen atom incorporated in the perovskite structure.

Keywords: perovskite, thermal stability, degradation of perovskites, structural transformations.

Термічна стабільність перовськітів $CH_3NH_3PbX_3$(X= Cl, Br ,I).

С.С. Смоляк, В.Л. Карбівський, В.Х. Касіяненко, С.А. Неділько, С.І. Шулима, Н.А. Курган, О.А. Пузько, Л.І. Карбівська, А.П. Сорока

Морфологію та структуру перовськітів досліджено за допомогою сканувальної електронної мікроскопії та рентгенівської дифракції. Показано, що структура зразків є монофазною. Досліджено термічну стабільність та процеси деградації при рівномірному нагріванні серії перовськітів $CH_3NH_3PbX_3$ (X= Cl, Br, I) за допомогою термогравіметричного аналізу. Визначено термічну стабільність до 335°C для X = Cl, до 330°C для X = Br, до 310°C для X = I. Встановлено залежність термічної стабільності перовськітів $CH_3NH_3PbX_3$ від природи атому галогену в їх структурі. За допомогою варіювання атому галогену с структурі перовськіту можна керувати термічною стабільністю гібридних органо-неорганічних перовськітів.

1. Introduction

The rising interest in perovskite materials is driven by their remarkable potential in various electronic applications, including photodetectors [1] and laser diodes [2, 3]. Furthermore, metal oxide perovskites play a vital role in catalysis [4]. In recent years, hybrid perovskite materials have gained popularity as a game-changing alternative for developing cost-effective and highly efficient solar cells [5]. Among these, halide perovskites stand out due to their low manufacturing costs and the prospects for their use as flexible solar cell technologies. Thanks to advances in interface design and improvements in the morphology of perovskite films, the efficiency of solar cells incorporating these materials has increased dramatically from just 3.9% in 2009 to an impressive 26.0% today [6].

However, the functionality of perovskites, particularly $CH_3NH_3PbX_3$ (X = Cl, Br, I), in practical environments faces a critical obstacle:

degradation. The main causes of degradation include chemical breakdown in humid conditions [7, 8, 9, 10], exposure to UV light [11, 12], and the effects of extreme temperatures [13, 14].

Temperature is an unavoidable stress factor that significantly impacts the performance of photovoltaic systems, leading to degradation over time. According to international standards, operational temperatures between 60°C and 85°C are deemed acceptable [15]. However, enhancing tolerance to higher temperatures is essential for applications in hot climates and technologies that may generate excessive heat during operation.

Therefore, solving these problems will unlock the full potential of perovskite materials $CH_3NH_3PbX_3$ (X= Cl, Br, I) in the energy sector, paving the way for innovative solutions and sustainable energy advancements.

However, data on the thermal degradation of hybrid perovskite materials are highly controversial; there are different interpretations regarding the chemical composition of the gases released during the thermal decomposition of perovskites $CH_3NH_3PbX_3$ (where X = Cl, Br, I).

In [16-18], based on thermal gravimetric analysis the authors suggested that during the initial mass loss of $CH_3NH_3PbI_3$, hydrogen iodide (HI) and methylamine (CH_3NH_2) are released sequentially. Conversely, the authors of [19, 20] utilized both thermal gravimetric analysis and Fourier-transform infrared spectroscopy (FTIR) and concluded that the perovskite decomposes with the release of ammonia (NH_3) and methyl iodide (CH_3I). This conclusion was further substantiated in [21] through the combination of thermal gravimetric analysis with mass spectrometry (MS). Furthermore, in [22], in addition to the primary gases NH_3 and CH_3I, methane (CH_4) was identified for the first time as a product of thermal degradation at elevated temperatures during the decomposition of $CH_3NH_3PbI_3$. The researchers noted that during the thermal degradation of $CH_3NH_3PbBr_3$, hydrogen bromide (HBr) and CH_3NH_2 are released [23]. It is important to emphasize that most studies in this field have been carried out in inert gas atmospheres, such as argon or nitrogen.

A deep understanding of the degradation mechanism is essential for addressing the limited service life of hybrid perovskite materials under operational conditions. Thus, the objective of this study was to investigate the thermal stability of perovskite materials $CH_3NH_3PbX_3$ (X = Cl, Br, I), paying special attention to their degradation upon uniform heating under conditions as close as possible to real operating conditions, namely, in an air atmosphere with free convection.

2. Experimental

Synthesis. The synthesis of the samples under investigation is illustrated using the example of polycrystalline $CH_3NH_3PbBr_3$ obtained by precipitation using hydrobromic acid, namely the the Poglitsch method [24]. In this procedure, 2.5 g of lead (II) acetate trihydrate (99.5 – 102.0%, ACS reagent, "Sigma Aldrich") was dissolved in 10 ml of concentrated aqueous HBr solution (48 wt.%). The mixture was then heated to a temperature of 90 °C. To this solution, 2 ml of concentrated hydrobromic acid was added, along with 0.597 g of methylamine (CH_3NH_2) in a 40 wt.% aqueous solution. After cooling the solution from approximately 90 °C to room temperature for 72 hours, orange crystals of about 2 mm in size formed. $CH_3NH_3PbX_3$ (where X = Cl, I) was synthesized using a similar precipitation method from appropriate solutions.

Thermal Analysis. Thermal analysis was carried out on a Derivatograph Q-1500 D (MOM, Budapest), with a steady heating rate of 10°C/min in a free air convection atmosphere in the temperature range from room temperature up to 800°C. For each measurement, platinum crucibles containing approximately 0.37 mg of sample material were used. The loss of mass of the sample upon heating was measured by thermogravimetry (TG); while differential thermogravimetry (DTG) was used to determine the rate of weight loss or gain upon heating, cooling or under isothermal conditions; its results are presented as the derivative of the change in mass with respect to temperature or time ($-dm/dt$). The DTG curve is the first derivative of the TG, and the peak height of the DTG curve corresponds to the rate of mass loss at any given temperature. Differential thermal analysis (DTA) assesses the temperature difference between a sample (T_S) and a reference (T_R). The $T_S - T_R$ graph over the programmed temperature range displays a series of peaks, indicating the temperatures at which various thermal processes occur. A relative error is 0.3%.

X-ray diffraction (XRD). X-ray investigations were conducted at room temperature using a Shimadzu LabX diffractometer XRD-6000 with CuK_α radiation (λ = 1.54178 Å).

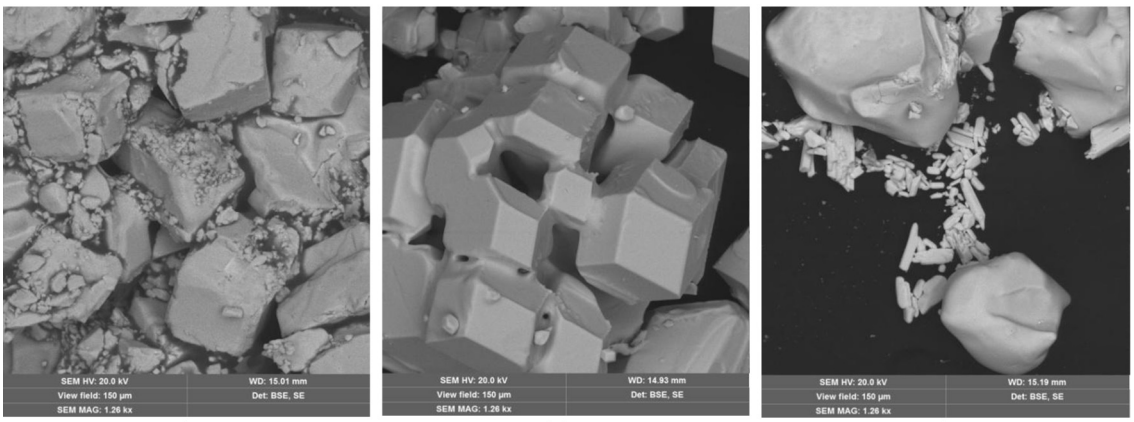

Fig. 1. Scanning electron microscope images of various perovskites a) $CH_3NH_3PbCl_3$, b) $CH_3NH_3PbBr_3$, c) $CH_3NH_3PbI_3$.

Diffraction spectra were recorded by θ-2θ scanning with Bragg-Brentano focusing in the range of 2θ angles from 5 to 70 degrees with a step of Δ(2θ) = 0.02 deg. The exposure time at each point was 1 second. The obtained samples turned out to be monophase.

Scanning electron microscopy (SEM). The perovskite morphology and elemental composition were analyzed using a Tescan Mira 3 microscope, allowing for precise imaging at accelerating voltages between 5 – 20 kV. We used the integrated Oxford X-max 80 mm² setup to obtain detailed energy dispersive X-ray (EDX) spectra, providing accurate and reliable results that expand our knowledge of these materials.

3. Results and discussion

According to recent SEM studies, the particles $CH_3NH_3PbCl_3$ and $CH_3NH_3PbBr_3$ have a remarkable cubic crystal structure (see Fig. 1a and 1b). In contrast, $CH_3NH_3PbI_3$ has a needle-like crystal morphology (see Fig. 1c), demonstrating the diversity in crystal forms among these compounds. Utilizing X-ray diffraction, it was confirmed that the synthesized samples are monophase perovskites of the form $CH_3NH_3PbX_3$ (where X = Cl, Br, I) with the corresponding stoichiometric composition. The diffractograms show no evidence of amorphous or impurity phases (see Fig. 2). Both $CH_3NH_3PbCl_3$ and $CH_3NH_3PbBr_3$ exhibit a cubic structure, while $CH_3NH_3PbI_3$ crystallizes in a tetragonal structure (refer to Table 1).

These structural differences result in different morphologies of the samples observed by scanning electron microscopy (SEM). The lattice parameters of the perovskites $CH_3NH_3PbX_3$ (X = Cl, Br, I), given in Table 1, are in good agreement with previously published data [17]. It is evident that the lattice parameters increase in accordance with the increase in the ionic radii of the halogen atoms: Cl (1.81 Å) → Br (1.96 Å) → I (2.20 Å).

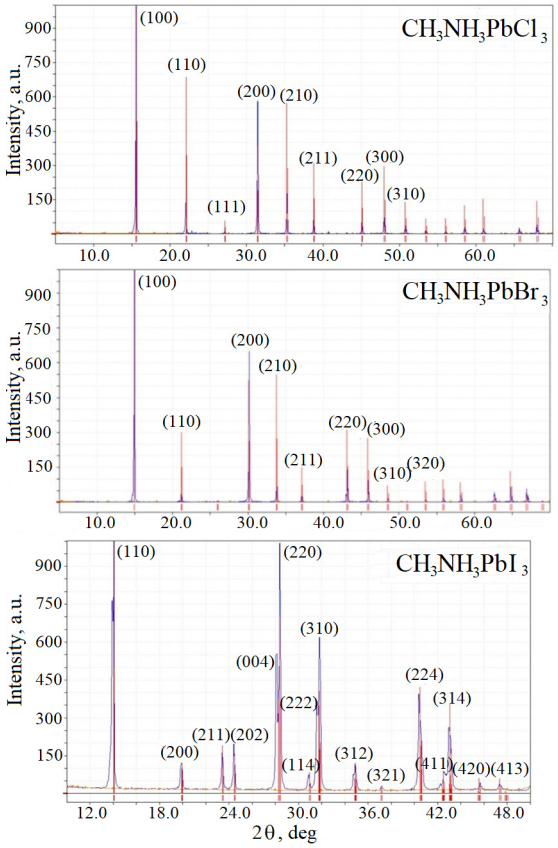

Fig. 2. The X-ray diffraction patterns of the perovskite compound $CH_3NH_3PbX_3$, where X = Cl, Br, I.

The elemental composition of perovskites $CH_3NH_3PbX_3$ (where X = Cl, Br, I) was analyzed using the EDX method (see Fig. 3). The analy-

Table 1. Results of X-ray diffraction studies on perovskites $CH_3NH_3PbX_3$ (X= Cl, Br, I)

Sample	Space group, crystal system	Unit cell parameters, Å
$CH_3NH_3PbCl_3$	P*m*3*m* (221) cubic	a = 5.68670 a = 5.68415 [17]
$CH_3NH_3PbBr_3$	P*m*3*m* (221) cubic	a = 5.93280 a = 5.93129 [17]
$CH_3NH_3PbI_3$	I4*cm* (108) tetragonal	a = 8.89210 c =12.60400 a = 8.8743 [17] c = 12.6708 [17]

sis revealed the presence of the chemical elements C, N, Pb, and Cl, Br, I, along with minor traces of O and Al. The detected O and Al in the EDX spectra can be attributed to residues from the synthesis reagents. Based on the EDX data, the ratio of the concentrations of elements Pb to X in the studied perovskites $CH_3NH_3PbX_3$ (X = Cl, Br, I) is close to the calculated value 1:3, namely Pb:Cl = 1:2.9; Pb:Br = 1:3.4; Pb:I = 1:3.3. The increased concentration of carbon is due to the peculiarities of fixing the samples on the holder during the experiment, while the absence of hydrogen is a consequence of the insensitivity of the method to light elements.

The thermal stability of $CH_3NH_3PbX_3$ (X = Cl, Br, I) was studied in air with heating at a steady constant rate of 10°C/min. Remarkably, no mass loss was detected in the samples up to 330°C for X = Br, up to 335°C for X = Cl, and up to 310°C for X = I. This is particularly noteworthy, especially in comparison with the work [25], which reported that perovskites with X = I and Br are stable up to 250°C and 300°C, respectively.

The TG/DTG/DTA parameters collected during our study of $CH_3NH_3PbX_3$ (X= Cl, Br, I) perovskites provide important information, detailed in Table 2.

$CH_3NH_3PbBr_3$. During heating, we observed a small peak at 60°C on the DTA curve (see Fig. 4). This peak is not accompanied by mass loss, likely signaling a structural distortion of the perovskite. However, our study did not analyze the intermediate products during the heating process to confirm this assumption. The DTG curves for $CH_3NH_3PbBr_3$, shown in Fig. 4, indicate that thermal stability is maintained up to 330°C, after which mass loss loss is initiated. The decay of perovskite can be represented by the following chemical reaction [23]:

$$CH_3NH_3PbBr_3 \leftrightarrow HBr + CH_3NH_2 + PbBr_2$$

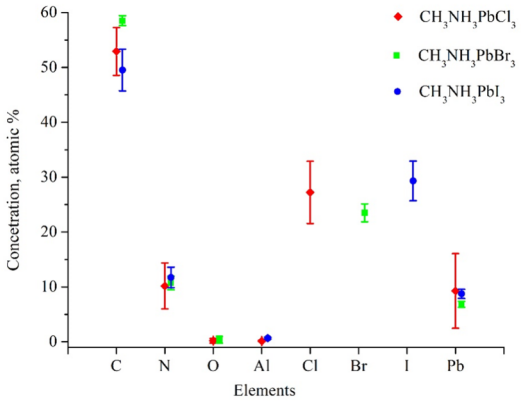

Fig. 3. The elemental analysis of the perovskite compound $CH_3NH_3PbX_3$, where X represents the halogens Cl, Br, and I.

The mass loss occurs in two successive stages, as indicated by the TG curve in Fig. 4, at approximately 380°C and 683°C (see Table 2). The first stage involves at least two intermediate stages of mass loss occurring at around 380°C and 470°C, each developing at different rates (as shown in the DTG curve in Fig. 4). The mass loss observed at 380°C is attributed to the initial decomposition of the perovskite, leading to the formation of the decomposition product HBr [23]. The subsequent mass loss is due to the breakdown of the organic component – methylamine. Above 683°C, $PbBr_2$ is generated. In contrast to [23], this study finds that the endothermic effects are shifted to higher temperature regions.

Ultimately, we found that the mass loss of the $CH_3NH_3PbBr_3$ perovskite material reached an impressive 95.5%.

$CH_3NH_3PbCl_3$. Figure 5 illustrates the results of the study on $CH_3NH_3PbBr_3$ subjected to uniform heating. Similar to the results for $CH_3NH_3PbBr_3$, the DTA curve shows a slight endothermic effect at around 60°C, suggesting

Table 2. Comprehensive Analysis of TG/DTG/DTA parameters for $CH_3NH_3PbX_3$ (X = Cl, Br, I) perovskites.

Materials	Thermal stability for,°C	DTA peaks, °C	DTG peaks, °C	Mass loss, %	Residual mass, %
$CH_3NH_3PbCl_3$	335	500 535 565 635 675	390 488	63.9	36.1
$CH_3NH_3PbBr_3$	330	370 630 740 800	380 470 683 763	19.1 76.4	0.5
$CH_3NH_3PbI_3$	310	365 390 510 540 605	365 390 450 510 605	10.2 82.3	7.5

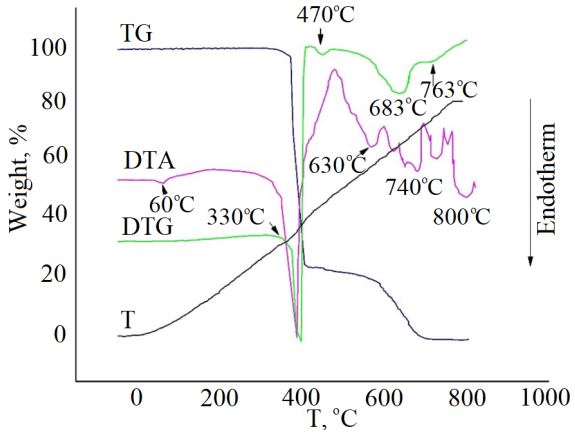

Fig. 4. Thermal behavior of TG (blue), DTA (violet), and DTG (green) of perovskite $CH_3NH_3PbBr_3$ at a heating rate of 10 °C/min in flowing air.

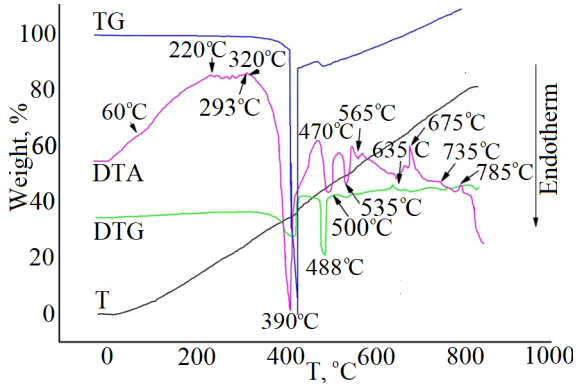

Fig. 5. The thermal behavior of TG (blue), DTA (violet), and DTG (green) of perovskite $CH_3NH_3PbCl_3$ with a heating rate of 10 °C/min in flowing air.

that the sample undergoes structural distortion in this temperature range. The DTA curve displays a series of peaks at 220°C, 240°C, 270°C, 279°C, and 290°C, which do not correlate with any changes in the sample mass, indicating the onset of phase transitions. Notable sharp changes begin on the DTA curve starting at 320°C, leading to a peak endothermic effect at 390°C. This peak is associated with the release of volatile substances, resulting in mass loss as seen in the TG curve. Overall, the analysis of the DTG curve for the perovskite $CH_3NH_3PbCl_3$ suggests that the sample loses mass in two stages, according to peaks observed at 390°C and 488°C, both accompanied by endothermic effects (heat absorption as indicated by the DTA curve). The initial stage corresponds to the loss of HCl and the organic component CH_3NH_2.

According to Figure 5, there is no mass loss detected in the temperature range of 500°C to 800°C. In fact, the TG curve shows a slight increase in mass, even though it is clear that the actual mass of the product cannot increase. Given the behavior of the TG curve, a detailed analysis of the peaks at 500°C, 535°C, 565°C, 635°C, 675°C, 735°C, and 785°C has not been performed. This observed effect was attributed to aerodynamic forces within the heating furnace, as described in [26]. Notably, this ef-

fect was characteristic only for the perovskite $CH_3NH_3PbCl_3$, since similar samples of $CH_3NH_3PbX_3$ (where X = Br, I) did not exhibit any significant mass increase.

$CH_3NH_3PbI_3$. Figure 6 presents the thermal analysis curves of the perovskite $CH_3NH_3PbI_3$. Similar to $CH_3NH_3PbBr_3$ and $CH_3NH_3PbCl_3$, the DTA curve (Figure 6) shows a small endothermic peak at 60°C, which is not associated with any mass loss. This peak may indicate the tetragonal-to-cubic phase transition, which is consistent with the results obtained in [19]. A transition for this compound was noted at 57°C in [27].

The mass loss of the examined perovskite begins at 310 °C, which is consistent with the results of studies [28, 29]; this indicates degradation of $CH_3NH_3PbI_3$ around 300 °C.

The thermogravimetric (TG) curve (Fig. 6) reveals the mass loss of the $CH_3NH_3PbI_3$ sample in two consecutive stages. During the first stage, two endothermic effects with peaks at 365 °C and 390 °C are observed in the DTA curve. These effects develop at slightly different rates, as evidenced by peaks at 365 °C, 390 °C, and 450 °C on differential thermogravimetry (DTG) curve. These peaks indicate the loss of HI and CH_3NH_2. In the temperature range of 510 °C to 650 °C, the PbI_2 phase forms as is formed as a decomposition product of $CH_3NH_3PbI_3$. The decomposition upon heating can be schematically represented as follows:

$$CH_3NH_3PbI_3 \leftrightarrow HI + CH_3NH_2 + PbI_2.$$

An alternative thermal degradation pathway for $CH_3NH_3PbI_3$ has been suggested in studies [19-22], involving the formation of $CH_3NH_3PbI_3 \leftrightarrow NH_3 + CH_3I + PbI_2$; however, we are inclined to believe that this process is not predominant for this perovskite. A similar conclusion was made in [30] that the decomposition to NH_3(g) and CH_3X(g), although thermodynamically favorable, appears to be seriously hampered by kinetic limitations associated with the breaking of the strong C–N bond in the organic cation.

The analysis of the data presented in the Table 2 indicates that $CH_3NH_3PbCl_3$ and $CH_3NH_3PbBr_3$ exhibit greater stability than $CH_3NH_3PbI_3$. This can be attributed to the characteristics of the halogen atoms within the perovskite structure. According to the Pauling electronegativity scale, chlorine displays a higher electronegativity compared to bromine and iodine (Cl = 3.0 → Br = 2.8 → I = 2.5), which enhances its ability to capture electrons. This property complicates the reduction of lead (Pb) to its zero oxidation state (Pb^0) and results in stronger ionic bonds in $CH_3NH_3PbCl_3$ compared to $CH_3NH_3PbBr_3$ and $CH_3NH_3PbI_3$. This conclusion is supported by similar studies [31], which show that the greater stability of $CH_3NH_3PbCl_3$ compared to $CH_3NH_3PbI_3$ and $CH_3NH_3PbBrI_3$ is due to stronger ionic character of the Pb-Cl bond. Furthermore, when comparing the ionic radii of the halogens in the examined perovskites, we observe the following increase: Cl = 1.81 Å, Br = 1.96 Å, and I = 2.20 Å. The presence of a halogen atom with a smaller radius in the structure $CH_3NH_3PbX_3$ (where X = Cl, Br, I) facilitates a more compact arrangement, suggesting that $CH_3NH_3PbCl_3$ should be the most stable. This conclusion is consistent with the observations in our study (see Table 2).

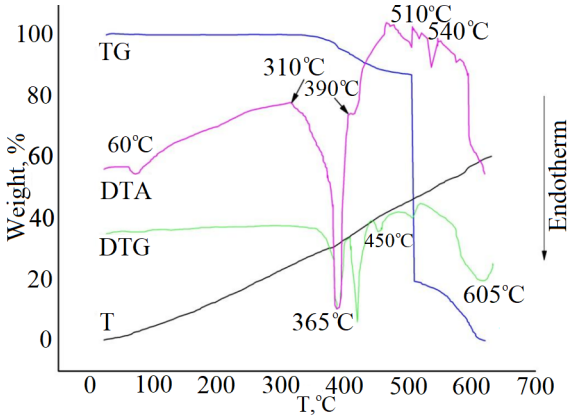

Fig. 6. The thermal behavior of TG (blue), DTA (violet), and DTG (green) for perovskite $CH_3NH_3PbI_3$ at a heating rate of 10 °C/min in flowing air.

4. Conclusions

Using X-ray diffraction (XRD) and scanning electron microscopy (SEM) techniques, it was established that $CH_3NH_3PbX_3$ perovskites (where X = Cl, Br) crystallize in a cubic system with space group P*m*3*m*. In contrast, $CH_3NH_3PbI_3$ crystallizes in a tetragonal structure with space group I4cm. Under uniform thermal heating at a rate of 10°C/min in air, the perovskites $CH_3NH_3PbX_3$ (X = Cl, Br, I) demonstrate stability up to 335°C for X = Cl, 330°C for X = Br, and 310°C for X = I. Beyond these temperatures, further uniform heating initiates decomposition processes in the samples, primarily occurring in two stages and resulting in mass loss. Thermogravimetric

analysis established a correlation between the stability of $CH_3NH_3PbX_3$ perovskites and the nature of the halogen atom. In particular, it was noted that the greater the electronegativity and the smaller the radius of the halogen atom incorporated into the perovskite structure, the higher the thermal stability of the compound. This study highlights that by changing the halogen atom within the perovskite structure, the thermal stability of hybrid organic-inorganic perovskites can be controlled.

Acknowledgement

This research was supported by National Academy of Sciences of Ukraine, Grant **"Solar cells based on perovskites and apatites"** (0123U100914).

References

1. Z. Yuan, W. Huang, S. Ma, W. Hu, and W. Zhang, *J. Mater. Chem.* C, **7**, 5442 (2019). https://doi.org/10.1039/C9TC00892F
2. C-H. Lin, C-Y. Kang, T-Z. Wu, C-L. Tsai, C-W. Sher, X. Guan, P-T. Lee, T. Wu, C-H. Ho, H-C. Kuo, J-H. He, *Adv. Funct. Mater.,* **30** 1909275 (2020). https://doi.org/ 10.1002/adfm.201909275
3. A.M. Al-Amri, B. Cheng, J-H. He, *IEEE Trans. Nanotechnol.,* **18**, 1 (2019). https://doi.org/ 10.1109/TNANO.2018.2872887
4. J. Hwang, R.R. Rao, L. Giordano, Y. Katayama, Y. Yu, Y. Shao-Horn, *Science,* **358**, 751 (2017). https://doi.org/10.1126/science.aam7092
5. J.-P. Correa-Baena, M. Saliba, T. Buonassisi et al., *Science*, **358**, 739 (2017). https://doi.org/10.1126/science.aam6323.
6. Rice University. "Lab achieves major gains in perovskite solar cell stability." ScienceDaily. ScienceDaily, 13 June 2024. <www.sciencedaily.com/releases/2024/06/240613221908.htm>.
7. F. Li and M. Liu, *J. Mater. Chem.* A, **5**, 15447 (2017). https://doi.org/10.1039/C7TA01325F
8. J. Yang, B.D. Siempelkamp, D. Liu, T.L. Kelly, *ACS Nano*, **9**, 1955 (2015). https://doi.org/: 10.1021/nn506864k
9. J.S. Manser, M.I. Saidaminov, Christians, J.A., et al., *Accounts of Chemical Research,* **49**, 330 (2016). https://doi.org/10.1021/acs.accounts.5b00455
10. N. Aristidou, I. Sanchez-Molina, et al., *Angew. Chemie - Int. Ed.*, **54,** 8208 (2015). https://doi.org/10.1002/anie.201503153
11. Xiuxiu Niu, Nengxu Li, Zhenhua Cui , Liang Li et al., *Advanced Materials*, **35**(45) e2305822 (2023). https://doi.org/10.1002/adma.202305822
12. T. Colenbrander, J. Peng, Y. Wu et al., *Energy Advances,* **2**, 298 (2023). https://doi.org/10.1039/d2ya00218c
13. V. Romano**,** A. Agresti, R. Verduci, G. D'Angelo, *ACS Energy Lett.,* **7**, 2490 (2022). https://doi.org/10.1021/acsenergylett.2c01099
14. A. W. Y. Ho-Baillie, H. G. J. Sullivan, T. A. Bannerman, H. P. Talathi, J. Bing, S. Tang, A. Xu, D. Bhattacharyya, I. H. Cairns and D. R. McKenzie, *Adv. Mater. Technol.*, **7**, 2101059 (2022). https://doi.org/10.1002/admt.202101059
15. https://www.fluxim.com/isos-protocols-stability-perovskite-solar-cells
16. A. Dualeh, P. Gao, S. I. Seok, M. K. Nazeeruddin, M. Grätzel, *Chem. Mater.*, **26**, 6160 (2014). https://doi.org/10.1021/cm502468k
17. B. Brunetti, C. Cavallo, A. Ciccioli, et al., *Sci Rep.*, **6**, 31896 (2016). https://doi.org/10.1038/srep31896
18. D. P. Nenon, J. A. Christians, L. M. Wheeler, J. L. Blackburn, E. M. Sanehira, B. Dou, M. L. Olsen, K. Zhu, J. J. Berry, J. M. Luther, *Energy Environ. Sci.,* **9**, 2072 (2016). https://doi.org/10.1039/C6EE01047D
19. A. E. Williams, P. J. Holliman, M. J. Carnie, M. L. Davies, D. A. Worsley, T. M. Watson, *J. Mater. Chem.* A, **2**, 19338 (2014). https://doi.org/10.1039/C4TA04725G
20. W. Yang, R. Shi, H. Lu, K. Liu, Q. Yan, Y. Bai, X-L. Ding, H. Li, Z. Gao, *Physical Chemistry Chemical Physics,* **26**, 17999 (2024). https://doi.org/:10.1039/D4CP01318B
21. E. J. Juarez-Perez, Z. Hawash, S. R. Raga, L. K. Ono and Y. Qi, *Energy Environ. Sci.*, **9**, 3406 (2016). https://doi.org/ 10.1039/c6ee02016J
22. L. Ma, D. Guo, M. Li, C. Wang, Z. Zhou, X. Zhao, F. Zhang, Z. Ao, and Z Nie, *Chem. Mater.*, **31**, 8515 (2019). https://doi.org 10.1021/acs.chemmater.9b03190
23. R. K. Singh, R. Kumar, A. Kumar, N. Jain, R. Kr. Singh, J. Singh, *Journal of Alloys and Compounds,* **743**, 728 (2018) https://doi.org/10.1016/j.jallcom.2018.01.355
24. A. Poglitsch, D. Weber, *The Journal of Chemical Physics,* **87**, 6373 (1987). https://doi.org/10.1063/1.453467
25. L. Dimesso, M. Dimamay, M. Hamburger, and W. Jaegermann, *Chem. Mater.*, **26**, 6762 (2014). https://doi.org/10.1021/cm503240k
26. R.J. Crewe, J.E.J. Staggs, P.T. Williams, *Polymer Degradation and Stability*, **92**, 2070 (2007). https://doi.org/10.1016/j.polymdegradstab.2007.07.023
27. T. Baikie, Y. Fang, J. M. Kadro, M. Schreyer, F. Wei, S. G. Mhaisalkar, M. Graetzel, Tim J. White, *Journal of Materials Chemistry* A, **1**, 5628 (2013). https://doi:10.1039/C3TA10518K

28. R. K. Singh, N. Jain, R. Kumar, in: Conference Paper in AIP Conference Proceedings, Bikaner, India (2018). DOI: 10.1063/1.5032825
29. D. Prochowicz, M. Franckevičius, A. M. Cieślak, S. M. Zakeeruddin, M. Grätzel, J. Lewinski, *J. Mater. Chem.* A, **3**, 20772 (2015). https://doi:10.1039/C5TA04904K
30. A. Ciccioli and A. Latini. *J. Phys. Chem. Lett.*, **9**, 3756 (2018). https://doi.org/10.1021/acs.jpclett.8b00463
31. H-P. Hsu, L-C. Li, M. Shellaiah, K. W. Sun, *Scientific Reports,* **9**, 13311 (2019). https://www.nature.com/articles/s41598-019-49926-z